2021 International Conference on Smart-Green Technology in Electrical and Information Systems (ICSGTEIS) | 978-1-6654-1355-8/21/$31.00 ©2021 IEEE | DOI: 10.1109/ICSGTEIS53426.2021.9650364

The Development of Laboratory-Scale Oscillating Water Column OWC Test Rig with Real-Time Data Monitoring System

Nurul Hiron
Department of Electrical Engineering
Siliwangi University
Indonesia
hiron@unsil.ac.id
https://orcid.org/0000-0003-0516-8278

Ida Ayu Dwi Giriantari
Department of Electrical Engineering
Udayana University
Indonesia
dayu.giriantari@unud.ac.id

Lie Jasa
Department of Electrical Engineering
Udayana University
Indonesia
liejasa@unud.ac.id

I Nyoman Satya Kumara
Department of Electrical Engineering
Udayana University
Indonesia
satya.kumara@unud.ac.id

Abstract— Oscillating water column (OWC) with vertical axis wind turbine (VAWT) involves extracting ocean waves into electrical energy. To know the performance of OWC with VAWT in depth requires a complex monitoring system. This article focuses on two discussions. The first is manufacturing the laboratory-scale OWC test rig, and the second is developing and validating the real-time monitoring system for the purpose-built OWC system. The monitoring system we proposed was consists of the sensors unit, MCU, and monitoring unit. The sensor unit is placed in certain parts of the test rig. And then, the measurement variables include wave oscillations, water surface oscillations in the chamber, rotation of the Savonius turbine in the OWC, air pressure in the chamber. The data acquisition uses the Arduino-Uno with graphics interface using the LabVIEW program. The test rig and the monitoring system have been successfully developed and tested on the OWC prototype with laboratory-scale VAWT. OWC and turbine performance measurement data have been successfully displayed in an interactive form and stored in data logging on a computer.

Keywords—OWC, energy, pressure, real-time monitoring system, turbine

I. INTRODUCTION

OWC is a wave energy converter (WEC) technology as we understand that the sea is an unlimited natural resource [1]. Besides OWC, several technologies can be applied to convert wave energy into electrical energy, such as power take-off (PTO) [2], Power buoy [3], Oscillating wave surge converter concept, Archimedes Wave Swing, and Wave Dragon. The OWC technology is getting more attention because of its design, which can replace the role of the breakwater as a controller of ocean wave energy [4]. Although the OWC has an efficiency of 29%, OWC has another essential function as a barrier to coastal abrasion caused by the sea [5], [6]. The efficiency of WEC technology is different for each type of WEC technology. For example, the pressure differential approach has been reported to work at 38% efficiency, the OWC with 29% efficiency, the overtopping mechanism with 17% efficiency, the oscillating body-heaving principle with 16% efficiency, and the oscillating body-Surging with 37% efficiency [3], [7], [8]. The OWC work system depends on the extraction of wave energy into mechanical energy. Therefore, it has become essential to exploring the energy extraction in OWC as a critical part of the wave power generation system.

The extraction of ocean waves into electrical energy in the OWC occurs through several stages. The first stage is wave collecting. The second stage is generating compressed air in the chamber. The third stage changes the air pressure into turbine rotation and converts the turbine's kinetic energy into electrical energy [9]. The study of energy extraction from waves has become an exciting topic of discussion to be explored. This study of energy conversion with OWC technology is based on the objective to explore renewable energy resources that is environmentally friendly. Therefore, in this respect, harnessing renewable energy sources such as wind, solar, and ocean wave energy has been the focus of researchers and practitioners [3]. Compared to photovoltaic technology, the OWC produces a much lower carbon footprint. In addition, the OWC technology helps observe coastal areas threatened by abrasion.

There are three approaches that researchers often use to determine the performance of an OWC system., The first is the simulation approach [10], the second is an experiment on the prototype [11], [12], and the third is a combination of simulation and experimental prototype [13]. Simulations with numerical computations are generally used to obtain detailed information about aerodynamic dynamics. The weakness of the simulation approach with mathematical models is that not all systems can be modeled in mathematical models. Therefore, it is necessary to complete additional data about the character of the material and external factors to obtain results that resemble actual conditions. The experimental approach with prototype can generally present the relationship of one part to another while still involving external variables. The experimental approach requires high accuracy sensors, high sampling time, and data acquisition tools integrated with the central computer unit (MCU). The simulation and prototype experiment are approaches that require complex systems and significant

Authorized licensed use limited to: UNIVERSITAS GADJAH MADA. Downloaded on January 26,2022 at 11:45:54 UTC from IEEE Xplore. Restrictions apply.

resources. This approach enables comparison of results to assist researchers in obtaining a reasonable results accuracy.

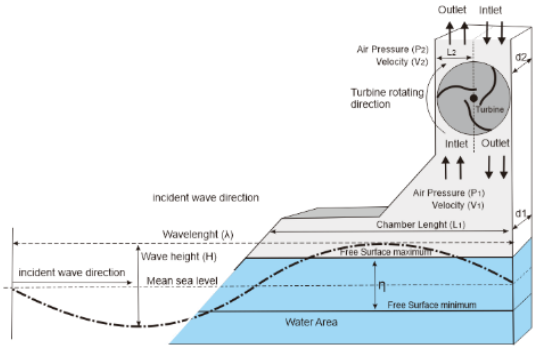

Fig. 1. OWC to convert wave to [36]

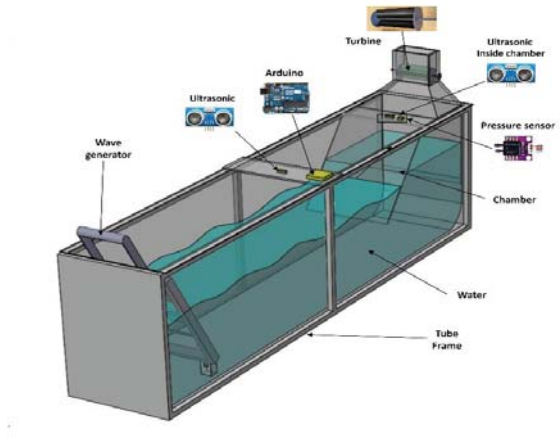

Fig. 2. Design of the laboratory-scale OWC test rig

An OWC design with VAWT has been raised as an exciting research theme by Dorrell et al. since 2004 [14]. This research then continued implementing the savonius turbine at the OWC [15]–[17]. The savonius study in a multi-chamber environment was conducted in-depth ocean wave energy extraction [18]–[20]. Many researchers conduct research studies by working on several simulation methods to create an Oscillating Water Column using a mathematical approach model [21]. In this method, there are limitations, namely using ideal data to produce an ideal system. A different method to avoid this is using a monitoring system to obtain direct data that can be applied to a prototype system that resembles the shape of the system in the field. In this system, there are two viewpoints in OWC operational. They are oscillation that occurs outside the chamber and oscillation that occurs inside the chamber. Then the chamber of OWC affects the turbine in converting potential energy into mechanical energy [22]. The outside will create an oscillatory motion of water that will produce the air pressure inside the chamber. The air pressure then produces a high airflow speed to rotate the wind turbine [23].

This paper focuses on studies to discover how wave energy extraction occurs in OWC involving VAWT turbines. To achieve this goal, a monitoring technique is needed that provides a clear and in-depth picture of the wind speed in the chamber, turbine speed, and how the relationship between wave oscillation energy and the energy generated is needed. This study was also implemented in an OWC environment [6] to obtain complete empirical data. A monitoring system and performance validation using a laboratory-scale OWC are carried out. Ni et al. conducted a similar study. [24]. However, the difference is that Ni et al.'s analysis focused on measuring the performance of a hydrofoil that operated close to a free surface over a range of angles of attack. The wave oscillations outside the chamber represent free seawater waves that will affect the oscillating water level in the chamber [25]. And then produces the kinetic power in the turbine and then the electrical power in the generator.

II. Material and Methods

A. Conceptual of OWC extraction

Fig. 1 is the concept of extracting ocean wave energy into kinetic energy in the turbine. Fundamentally, OWC operates in two conditions, namely a compressed state and a decompressed state. Compressed conditions occur when the incident wave (H) is in a high position so that the air pressure becomes (P1) high, then the airflow velocity (V1) is high. The compressed and decompressed condition then causes the turbine to rotate in one direction. The decompressed state is when H and P1 are very low, causing the airflow velocity (V2) to be high, then the turbine will rotate in the same direction during the compressed condition. The smaller the wavelength (λ) and the higher (H), the higher the value of V2 [6]. This condition is caused by the occurrence of water oscillations in the chamber that occur at high frequencies.

Fig. 5 Shows the proposed OWC test rig prototype designs on a laboratory scale. The prototype consists of four main parts. 1). water tube, 2) wave generator, 3) OWC chamber, 4) turbine. The wave generator is made from metal with a hand handle to swing the wave generator. The primary purpose of our manual wave generator is to easily generate the various wave with various periods so that the dynamic data can be created in the system. The water tube is an observation environment, and a wave generator is a tool for creating water waves. The chamber is a part of converting wave energy into mechanical energy [26]. The turbine is a part of the mechanical energy conductor to the generator. Our observation focused on turbine monitoring in the dynamic characteristics of OWC, so we decided not to involve the generator in this chase. The dimensions of the prototype are 2000 mm long, 600 mm wide, and 1000 mm high. We use acrylic and metal for the water tube, full acrylic for the OWC, and ABS+ for the turbine made by a 3D printer. The turbine and transducer positions are located as shown in Fig. 5.

B. Energy conversion procedure in OWC

As explained in section 1, OWC is concerned with converting wave energy into potential and kinetic energy. PE is the wave potential energy (joules) calculated using (1), KE is the wave kinetic energy (joules) using (2), Total wave energy (E_w) using (3). W=wave width (meters), assumed to be the same as chamber area in OWC (m), = density of water (kg/m^3), g=gravity (m/s^2), = wavelength (m), The H is height wave (cm). H and values are obtained from the water wave data captured by the ultrasonic sensor. E_w is the total wave energy in the chamber (watts), P_w is the wave power generated (watts). The Pw was calculated using (4) [27].

$$P.E = \frac{1}{4} w \rho g H^2 \lambda \, (J) \qquad (1)$$

Authorized licensed use limited to: UNIVERSITAS GADJAH MADA. Downloaded on January 26,2022 at 11:45:54 UTC from IEEE Xplore. Restrictions apply.

$$K.E = \frac{1}{4} w\rho g H^2 \lambda \, (J) \tag{2}$$

$$E_w = P.E + K.E = \frac{1}{2} w\rho g H^2 \lambda \, (J) \tag{3}$$

$$P_w = \frac{E_w}{T} = \frac{1}{2T} w\rho g H^2 \lambda \, (Watt) \tag{4}$$

$$V_2 = \frac{A_1}{A_2} V_1 = \frac{A_1}{A_2} \left| \frac{d\eta}{dt} \right| (m/s) \tag{5}$$

$$P_T = \tau \, \omega \, (Watt) \tag{6}$$

$$\tau = I_{\text{total}} \, \alpha \, (\text{Nm}) \tag{7}$$

$$\omega = 2\pi f \, (\text{rad/s}) \tag{8}$$

$$C_p = \frac{P_T}{(P_a + P_{AP})} \, (\text{Watt}) \tag{9}$$

$$P_a = \frac{1}{2} \rho A v^3 \, (\text{Watt}) \tag{10}$$

$$\text{TSR} = \frac{v_t}{v_a} = \frac{r\omega}{v_a} \tag{11}$$

$$P_{AP} = \left\{ \left(P_1 + \left(\frac{1}{2} \rho V_1^2 \right) \left(1 - \left(\frac{A_1}{A_2} \right)^2 \right) - P_0 \right) (V_2 A_2) \right\} \tag{12}$$

Chamber is the part that converts wave energy into mechanical energy [26]. The airflow velocity in the turbine chamber is proportional to the velocity of the water surface elevation in the chamber (η) times the ratio of the area of A1 to A2. Bernoulli's law applies to the calculation of air velocity V2 with equation (5) as in [17].

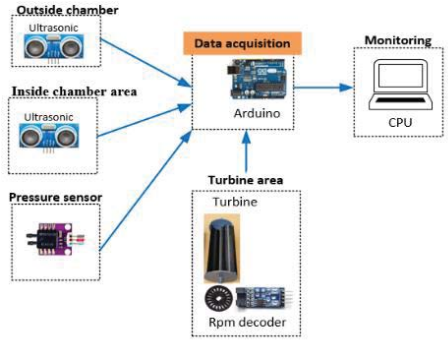

Fig. 3. Monitoring system architecture

The power produced by the turbine (Pt) can be calculated using equation (6). is turbine torque (N.m) and is turbine rotation speed (rpm). Turbine torque can be calculated by equation (7), where the I is the product of the moment of inertia (Kg.m^2) and the change in velocity (rad/s). The turbine has a moment of inertia on the shaft or rotating shaft of the turbine (Ishaft), the moment of inertia on the cover (I_{cover}), and the moment of inertia on the blades (I_{blade}). The calculation of the turbine moment inertia sequentially uses equations (8), (9), and (10), where the inertia is affected by the mass of the object (m) and the radius for the cylinder (R), the diameter for the blades (D). The total moment of inertia (Itotal) is the sum of all the inertia in the turbine as in equation (11) [28].

Naturally, energy extraction in the OWC system is not all of the wave power extracted into wind power. And not all of it will be converted into mechanical power. Some are lost due to aerodynamic drag on the turbine [29]. Turbine performance efficiency can be formulated as [23]. Turbine power coefficient (Cp) is calculated using equation (12). Cp is the ratio of PT to wind power (Pa) and air pressure power (P_{AP}), A is the turbine sweep area (m^2). Equation (14) is the TSR which is V_t is the ratio of turbine speed (m/s). The V_a is airspeed (m/s). P_{AP} in equation (15) is air pressure power, which has been discussed in detail in [23], and the Pin is the sum of air pressure power (P_{AP}) and wind power (Pa).

C. Monitoring system design

Fig. 4 is the monitoring system architecture on the OWC test rig is divided into several main parts with the installation position and the corresponding data capture function. As explained in the OWC structure in Fig. 2, the capture of wave oscillations outside the chamber and oscillations inside the chamber is sensed by ultrasonic sensor HC-SR04. HC-SR04 has an absolute error of ~0.035 cm/cm and a Precision standard deviation of ~0.1-0.5 cm. The measurement range is 2 cm to 450 cm [30], [31], [32] is a sufficient range to measure wave oscillations in the OWC. We used the rated speed of sampling data in 10 kHz for good results purposed in sampling data. The measurement results are presented in a graphical unit interface (GUI) system with Labview [33].

The air pressure in the chamber is captured using a bidirectional air pressure sensor MPXV7002 with a pressure arrange of -2 to 2 Kpa [34], [35]. Turbine rotation measurement using photodiode LM393 speed sensor and using (5). Dimensions of the OWC section we proposed as shown in Table I.

TABLE I. OWC PROTOTYPE SPECIFICATION

Part	Section	Value (unit)
Water tube	Long	200cm
	Wide	60cm
	High	100cm
Turbine	Blade long	22 cm
	Blade wide	4.7 cm
	Blade diameter	9.4 cm
	Blade mass	22.423 gram
	Shaft mass	6.932 gram
	Shaft radius	0.9 cm
	Blade mass	24.249 gram
	Blade radius	4.9 cm
Chamber	Chamber long	40 cm
	Chamber Wide	52 cm
	Chamber is (A1)	0.2 m^2
Turbine room (air inlet/outlet)	Wide (A2)	0.01 m^2

III. RESULT AND DISCUSSION

The integration of Arduino and the Labview Program makes it easy to organize interactive monitoring displays. At the same time, the Arduino-Uno with a sampling rate of at least 10 kHz provides data processing that is quite capable of handling changes from the data received from the sensor. Fig. 5 is a block diagram for processing data from ultrasonic sensors and then displaying accident wave oscillation data outside and inside the chamber, wave energy, wind power, airspeed, the power inside the chamber. Fig. 6 is a block diagram for processing data from ultrasonic sensors and

Authorized licensed use limited to: UNIVERSITAS GADJAH MADA. Downloaded on January 26,2022 at 11:45:54 UTC from IEEE Xplore. Restrictions apply.

displaying turbine RPM, power turbine, CP, TSR, electrical power. Fig. 7 to process and display PE, KE, EW, and power graph values.

Prototype OWC test rig in laboratory-scale has been successfully designed and built as shown in Fig. 4. According to Table I, the turbine (Fig. 2) is placed in the upper position of the chamber as Fig. 1. The dimensions of the A2 area are the same as 5% of the chamber area (A1). The placement of sensor units, data acquisition devices, and Graphic Unit Interfaces (GUI) must consider the risk of splashing water from waves in the unit tube. The tube unit as the water container contains the wave generator and OWC. At the top of the unit, the tube is placed in the sensor unit. Data acquisition devices are placed at the top, and the GUI uses a computer unit placed separately via a data cable.

Our test is carried out by filling water in a 60 cm high turbine, and then the wave is generated by moving it manually with a wave generator module. The monitoring system works and displays the measurement data as shown in Fig. 9 and Fig. 10. the displays a graph measuring turbine speed and power conversion (CP) and TSR. The information data in RMS turbine rotation, power, and efficiency can also be displayed in real-time. Fig. 9 displays a graph of wave energy, turbine energy, and electrical energy estimation measurement results. Data information in RMS units of energy in mechanical units is also displayed in the form of numbers. Fig. 9 displays a graph is measuring accident waves, water oscillations in the chamber, and air pressure. In addition, data in RMS units are also displayed in the form of numbers.

Fig. 10 is a graph of accident wave oscillations and water oscillations in the chamber. It appears that the accident wave has a dominant-negative value rather than a positive value. The accident wave range is -6 cm to 1 cm. While the oscillations in the chamber appear, positive values are proportional to negative values with a range of values between -6 cm to 6 cm. The conclusion from Fig. 10 is that although the accident waves tend to be irregular or random waves occur, the oscillations of the water surface in the chamber occur regularly. This finding confirms that the chamber will produce normal air pressure. The oscillatory velocity of the water surface in chamber V1 and the linear velocity of the wind flow in the turbine chamber (V2) are shown in Fig. 11. It appears that the airspeed of V1 has the same behavior as V2. Using equation (5) with equation (5), the average velocity of V2 is 2.42 m/s. The average speed of V1 is 0.12 m/s.

Fig. 12 shows a graph of the power produced by the chamber, which consists of air pressure power and wind power. Both of these powers are potential power to rotate the turbine blades. It appears that the air pressure power is greater than the wind power because the wave oscillations cause the high air pressure in the chamber. Based on Fig. 12, the average turbine power is 2.4 Watt, and the average wind power is 0.11 watts. This value is calculated using equation (13).

Fig.13 shows the relationship between turbine rotation and air pressure in the chamber. It appears that the turbine begins to rotate when the air pressure in the chamber begins to increase. When the wave starts to fall, the turbine rotation is still at high rotation, and this condition is due to the residual force, which causes the turbine centrifugal force. The monitoring system recorded that the average turbine rotation was 313.4 rpm while Pascal's air pressure range was (-83 Pa to 83 Pa).

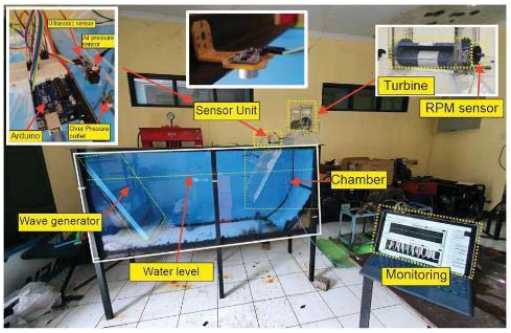

Fig. 4. Prototype OWC test rig in laboratory-scale

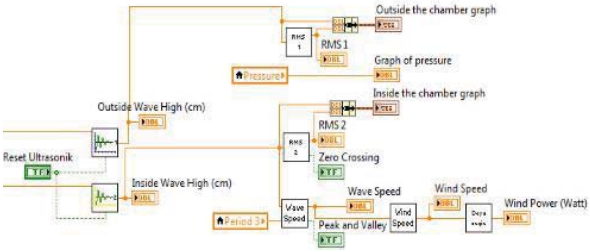

Fig. 5. Labview block diagram for wave energy data acquisition

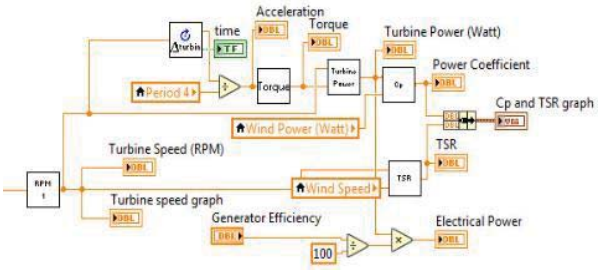

Fig. 6. Labview block diagram for turbine data aquisition

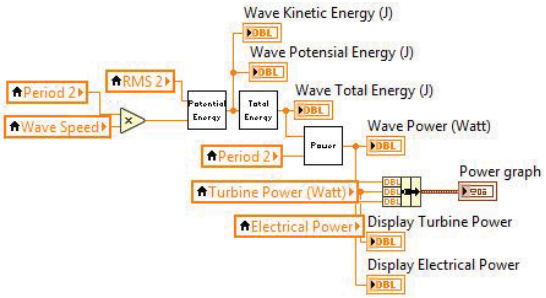

Fig. 7. Labview block diagram for energy monitoring

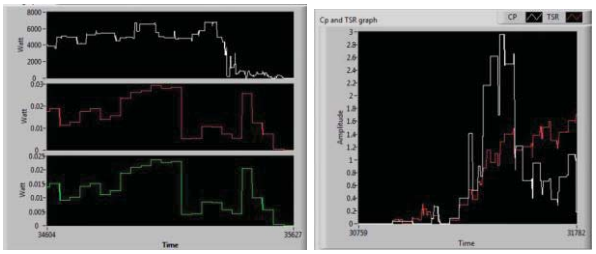

(a) (b)

Fig. 8. (a) Kinetic energy and potential energy. (b) CP vs TSR

Authorized licensed use limited to: UNIVERSITAS GADJAH MADA. Downloaded on January 26,2022 at 11:45:54 UTC from IEEE Xplore. Restrictions apply.

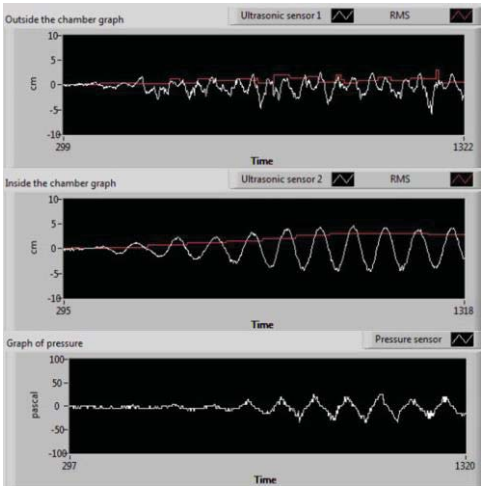

Fig. 9. Air Pressure and osillating wave capture display

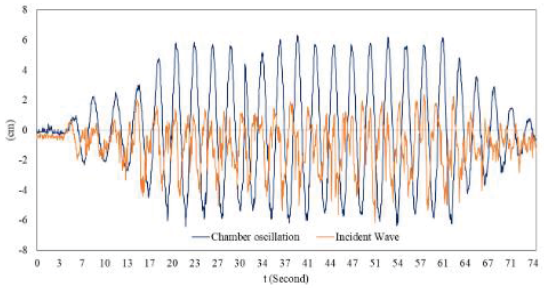

Fig. 10. Wave inside chamber and incident wave characteristic

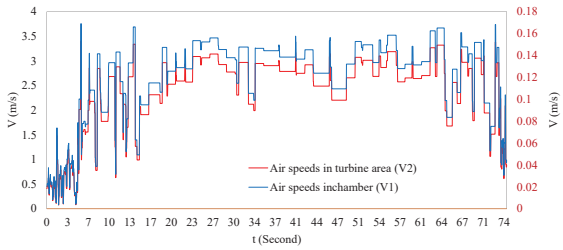

Fig. 11. Air speed V1 and V2

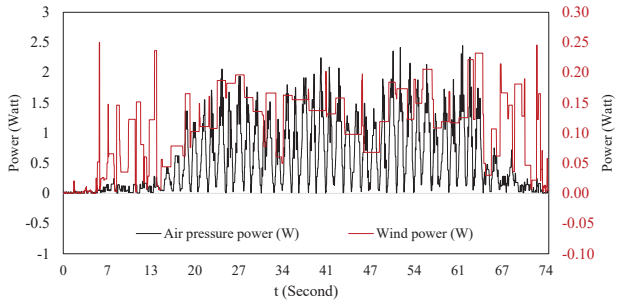

Fig. 12. Power turbine and wind power

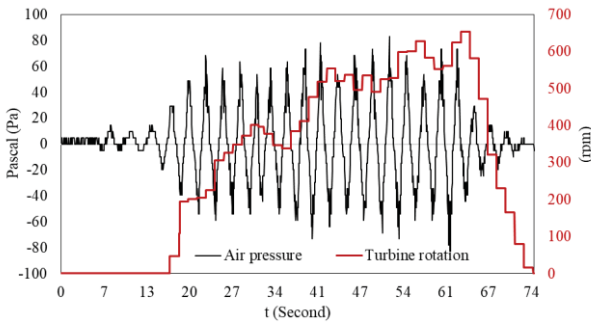

Fig.13. Air pressure dan turbine rotation

IV. Conclusion

This paper has discussed developing the laboratory-scale oscillating water column OWC test rig with a real-time data monitoring system. The monitoring system and the test rig have been successfully designed and tested. Data acquisition from the OWC and turbine work systems can use the ultrasonic sensor HC-SR04 bidirectional air pressure MPXV7002, Arduino Uno. Arduino Uno can overcome the sampling rate required in data acquisition. A Labview program to display monitoring results has been developed to provide an interactive display. Measuring the results and data loggers provides detailed information about wave oscillations and oscillations of the water surface in the chamber. The test result shows that the ratio A1 to A2 was 20, caused the air velocity to increase from 0.12 m/s in the chamber area to 2.42 m/s in the turbine area. The turbine model we proposed has a rotation maximum of 313.4 rpm or, in mechanic terms, was 2.4 watts.

Acknowledgment

This article was written as part of my Ph.D. research University of Udayana (UNUD) in Bali, Indonesia. This research was also supported by the Silwiangi University (UNSIL) of East Java.

References

[1] N. Hiron, A. Andang, and N. Busaeri, “Investigation of Wireless Communication from Under Seawater to Open Air with Xbee Pro S2B Based on IEEE 802.15.4 (Case Study: West Java Pangandaran Offshore Indonesia),” in Advances in Intelligent Systems and Computing, vol. 881, 2019, pp. 672–681.

[2] S. J. Kim, W. Koo, and M. H. Kim, “The effects of geometrical buoy shape with nonlinear Froude-Krylov force on a heaving buoy point absorber,” Int. J. Nav. Archit. Ocean Eng., vol. 13, pp. 86–101, 2021, doi: 10.1016/j.ijnaoe.2021.01.008.

[3] D. Qiao, R. Haider, J. Yan, D. Ning, and B. Li, “Review of wave energy converter and design of mooring system,” Sustain., vol. 12, no. 19, pp. 1–31, 2020, doi: 10.3390/su12198251.

[4] Empung, H. Nurul, and A. Chobir, “Oscillating Water Column (OWC) Building Performance Analysis as Beach Abrasion Reducing,” IIOAB J., vol. 7, no. Sopplement Issue, pp. 515–520, 2016, [Online]. Available: www.iioab.org.

[5] Empung, H. Nurul, and A. Chobir, “Oscillating Water Column (OWC) Building Performance Analysis as Beach Abrasion Reducing,” IIOAB J., vol. 7, no. Sopplement Issue, pp. 515–520, 2016, [Online]. Available: www.iioab.org.

[6] N. Hiron, I. A. D. Giriantari, L. Jasa, and I. N. S. Kumara, “The Performance of a Three-blades Fish-ridge Turbine in an Oscillating Water Column System for Low Waves,” in 2019 International Conference on Sustainable Engineering and Creative Computing (ICSECC), Aug. 2019, pp. 30–35, doi: 10.1109/ICSECC.2019.8907013.

Authorized licensed use limited to: UNIVERSITAS GADJAH MADA. Downloaded on January 26,2022 at 11:45:54 UTC from IEEE Xplore. Restrictions apply.

[7] A. Babarit, F. Wendt, Y. H. Yu, and J. Weber, “Investigation on the energy absorption performance of a fixed-bottom pressure-differential wave energy converter,” Appl. Ocean Res., vol. 65, pp. 90–101, 2017, doi: 10.1016/j.apor.2017.03.017.

[8] A. Babarit, “A database of capture width ratio of wave energy converters To cite this version : HAL Id : hal-01145072 A database of capture width ratio of wave energy converters,” 2019.

[9] N. Hiron, I. A. D. Giriantari, L. Jasa, and I. N. S. Kumara, “The Performance of a Three-blades Fish-ridge Turbine in an Oscillating Water Column System for Low Waves,” 2019, doi: 10.1109/ICSECC.2019.8907013.

[10] M. García-Díaz, B. Pereiras, C. Miguel-González, L. Rodríguez, and J. Fernández-Oro, “CFD Analysis of the Performance of a Double Decker Turbine for Wave Energy Conversion,” Energies, vol. 14, no. 4, p. 949, 2021, doi: 10.3390/en14040949.

[11] S. Doyle and G. A. Aggidis, “Experimental investigation and performance comparison of a 1 single OWC, array and M-OWC,” Renew. Energy, vol. 168, pp. 365–374, May 2021, doi: 10.1016/j.renene.2020.12.032.

[12] J. Kim and I. H. Cho, “Wave power extraction by multiple wave energy converters arrayed in a water channel resonator,” Int. J. Nav. Archit. Ocean Eng., vol. 13, pp. 178–186, 2021, doi: 10.1016/j.ijnaoe.2021.02.004.

[13] M. García-Díaz, B. Pereiras, C. Miguel-González, L. Rodríguez, and J. Fernández-Oro, “Design of a new turbine for OWC wave energy converters: The DDT concept,” Renew. Energy, vol. 169, pp. 404–413, May 2021, doi: 10.1016/j.renene.2020.12.125.

[14] D. G. Dorrell, J. R. Halliday, P. Millcr, and M. Findlater, “Review of wave energy resource and oscillating water column modelling,” in UPEC 2014. 39th International Universities Power Engineering Conference, 2004, vol. 1, pp. 649–653.

[15] M.-F. Hsieh, I.-H. Lin, D. G. Dorrell, M.-J. Hsieh, and C.-C. Lin, “Development of aWave Energy Converter Using a Two Chamber OscillatingWater Column,” IEEE Trans. Sustain. Energy, vol. 3, no. 3, pp. 482–497, 2012.

[16] D. G. Dorrell, M. F. Hsieh, and C. C. Lin, “A Small Segmented Oscillating Water Column Using a Savonius Rotor Turbine,” IEEE Trans. Ind. Appl., vol. 46, no. 6, pp. 2372–2380, 2010, doi: 10.1109/TIA.2010.2072979.

[17] M. Shalby, D. G. Dorrell, and P. Walker, “Multi–chamber oscillating water column wave energy converters and air turbines: A review,” Int. J. Energy Res., vol. 43, no. 2, pp. 681–696, 2019, doi: 10.1002/er.4222.

[18] D. G. Dorrell, M.-F. Hsieh, and C.-C. Lin, “A Multichamber Oscillating Water Column Using Cascaded Savonius Turbines,” IEEE Trans. Ind. Appl., vol. 46, no. 6, pp. 2372–2380, Nov. 2010, doi: 10.1109/TIA.2010.2072979.

[19] D. G. Dorrell and M. Hsieh, “Performance of Wells Turbines for use in Small-Scale Oscillating Water Columns,” in Proceedings of the 18th 2008 International Offshore and Polar Engineering Conference, 2008, pp. 393–400, [Online]. Available: http://citeseerx.ist.psu.edu/viewdoc/download?doi=10.1.1.846.9814&rep=rep1&type=pdf.

[20] M. Shaliby, P. Walker, and G. D. Dorrell, “The Investigation of Segmen Multi-Chamber Oscillating Water Column in Physical Scale Model,” Renew. Energy Res. Appl. (ICRERA), 2016 IEEE Int. Conf., vol. 5, pp. 3–8, 2016, doi: 10.1109/ICRERA.2016.7884534.

[21] P. Parjiman, M. Subekti, D. Daryanto, and M. Rif’an, “Simulasi Gelombang Laut Untuk Pembangkit Listrik Tenaga Gelombang Laut (PLTGL),” J. Teknol. Elektro, vol. 9, no. 2, 2015.

[22] V. Baudry, A. Babarit, and A. H. Clément, “An Overview of Analytical , Numerical and Experimental Methods for Modelling Oscillating Water Columns,” EWTEC 2013 Proc., 2013, doi: https://hal.archives-ouvertes.fr/hal-01158853.

[23] S. Deshmukh and S. Charthal, “Design and Development of Vertical Axis Wind Turbine,” IRA-International J. Technol. Eng. (ISSN 2455-4480), vol. 7, no. 2 (S), p. 286, 2017, doi: 10.21013/jte.icsesd201728.

[24] Z. Ni, M. Dhanak, and T. chow Su, “Performance of a hydrofoil operating close to a free surface over a range of angles of attack,” Int. J. Nav. Archit. Ocean Eng., vol. 13, pp. 1–11, 2021, doi: 10.1016/j.ijnaoe.2020.11.002.

[25] A. El Barakaz and A. El Marjani, “Analysis of Aero-hydrodynamic Equations Inside an OWC Device for Wave Energy Conversion,” 2017 Int. Renew. Sustain. Energy Conf., vol. 1, pp. 1–6, 2017.

[26] S. EL BOUJI, Z. BEIDOURI, and N. KAMIL, “Design and Optimization of an Oscillating Water Column Wave Energy Converter,” 2019 Int. Conf. Comput. Sci. Renew. Energies, pp. 1–3, 2019, doi: 10.1109/iccsre.2019.8807608.

[27] Empung, N. Hiron, and A. Chobir, “OSCILLATING WATER COLUMN (OWC) BUILDING PERFORMANCE ANALYSIS AS BEACH ABRASION REDUCING,” IIOAB J., vol. 7, no. 1, pp. 515–520, 2016.

[28] S. Subagyo and B. Basir, “Performance Analysis of Savonius Wind Turbine Without and With Vertical Stator Assembly,” no. March 2020, pp. 57–69, 2019, doi: 10.30536/p.siptekgan.2019.v23.07.

[29] J. Agbormbai and W. Zhu, “Experimental study of the performance of a novel vertical-axiswind turbine,” Appl. Sci., vol. 10, no. 8, 2020, doi: 10.3390/APP10082902.

[30] A. Andang, N. Hiron, A. Chobir, and N. Busaeri, “Investigation of ultrasonic sensor type JSN-SRT04 performance as flood elevation detection,” IOP Conf. Ser. Mater. Sci. Eng., vol. 550, no. 1, 2019, doi: 10.1088/1757-899X/550/1/012018.

[31] N. I. Abdulkhaleq, I. J. Hasan, and N. A. J. Salih, “Investigating the resolution ability of the HC-SRO4 ultrasonic sensor,” IOP Conf. Ser. Mater. Sci. Eng., vol. 745, no. 1, 2020, doi: 10.1088/1757-899X/745/1/012043.

[32] V. A. Zhmud, N. O. Kondratiev, K. A. Kuznetsov, V. G. Trubin, and L. V. Dimitrov, “Application of ultrasonic sensor for measuring distances in robotics,” J. Phys. Conf. Ser., vol. 1015, no. 3, 2018, doi: 10.1088/1742-6596/1015/3/032189.

[33] M. Schwartz and O. Manickum, Programming Arduino with LabVIEW. 2015.

[34] NXP Semiconductors, “Integrated Silicon Pressure Sensor On-Chip Signal Conditioned , Temperature Compensated and Calibrated SERIES,” Time, no. 2. pp. 1–9, 2012.

[35] T. D. E. Silva, V. Cabreira, and E. P. de Freitas, “Development and testing of a low-cost instrumentation platform for fixed-wing uav performance analysis,” Drones, vol. 2, no. 2, pp. 1–14, 2018, doi: 10.3390/drones2020019.

[36] N. Hiron, I. A. D. Giriantari, L. Jasa, and I. N. S. Kumara, “Fish-ridge wind turbine aerodynamics characteristics in Oscillating Water Column (OWC) system,” Ocean Syst. Eng., vol. 11, no. 2, pp. 141–159, 2021, doi: http://dx.doi.org/10.12989/ose.2021.11.2.141.

Authorized licensed use limited to: UNIVERSITAS GADJAH MADA. Downloaded on January 26,2022 at 11:45:54 UTC from IEEE Xplore. Restrictions apply.